



PERGAMON

Journal of Structural Geology 23 (2001) 1997–2009

**JOURNAL OF
STRUCTURAL
GEOLOGY**

www.elsevier.com/locate/jstrugeo

Oblique slip and the geometry of normal-fault linkage: mechanics and a case study from the Basin and Range in Oregon

Juliet G. Crider*

Department of Geology, Bryn Mawr College, Bryn Mawr, PA 19010, USA

Received 25 February 1999; accepted 3 March 2001

Abstract

Map patterns of normal fault linkages near Summer Lake, Oregon, show a systematic relationship between échelon step-sense, oblique-slip sense, and the position of linking faults. Where the step sense is the same as the sense of oblique slip (e.g. left step and left-oblique slip), the faults are linked in the lower part of their relay ramp. Where the step-sense and slip-sense are opposite (e.g. left-step and right-oblique slip), the faults are linked in the upper part of the ramp. A boundary-element code is used to calculate the stress field around échelon normal faults during oblique slip, and the model results reveal a relationship similar to the field observations. If step sense and oblique-slip sense are the same, there is a greater potential for deformation ahead of the tip of the front fault and in the lower part of the ramp. If step sense and oblique-slip sense are opposite, there is a greater potential for deformation ahead of the tip of the rear fault and in the upper part of the ramp. The field-model comparison confirms that oblique slip modifies the mechanical interaction among fault segments and thus influences fault growth and the geometry of fault linkage. © 2001 Elsevier Science Ltd. All rights reserved.

Keywords: Oblique slip; Normal fault linkage; Relay ramp

1. Introduction

Oblique extension is important in many rift systems, including the North Sea (Bartholomew et al., 1992; Oudmayer and de Jager, 1992; Faerseth et al., 1997), the Rio Grande Rift (Baldrige et al., 1994; Chapin and Cather, 1994), and the East African Rift System (Chorowicz and Sorlien, 1992; Scott et al., 1992). Each of these normal fault systems has a complex fault pattern that displays segmentation, faults arranged en échelon, and composite faults with zigzag traces. Oblique slip is also important in the Basin and Range of North America, where deviations from pure dip-slip are observed in both active normal faults (Caskey et al., 1996) and Tertiary structures (Fridrich et al., 1999).

Much of the previous research regarding oblique extension has been conducted using analog experiments, in which the boundary conditions are controlled and the evolution of the miniature fault systems can be directly observed. Freund and Merzer (1976), working with wet Portland cement, demonstrate that zigzag patterns are routine in extensional

systems. Smith and Durney (1992) show that échelon arrays of normal faults can be produced in clay during both orthogonal and oblique extension. They conjecture that echelon normal faults produced under rift-normal extension are precursors to a normal fault system with a zigzag map trace. Based on the results of their analog experiments in clay, Withjack and Jamison (1986) produced a widely-applied kinematic model for interpreting fault patterns created under oblique extension (see Pezzopane and Weldon, 1993; Umhoefer and Stone, 1996). Bonini et al. (1997) investigate successive oblique and orthogonal extension events in sand models, documenting that échelon oblique-normal faults form under oblique extension. Higgins and Harris (1997) and Richard (1991) study the formation of faults in clay cover-materials concurrent with oblique reactivation of rigid, underlying basement structures. Both studies report initiation of échelon oblique-slip faults. This happens even if the clay cover is decoupled from the rigid basement by a plastically-deforming layer (Higgins and Harris, 1997). Most importantly for the work presented here, Higgins and Harris (1997) describe the sequential development of structures in map pattern, beginning as échelon oblique-normal fault segments, that, with increasing extension, link to form continuous faults with irregular (zigzag) traces. All of these analog modeling examples produce zigzag map patterns under *non*-homogeneous stress

* Present address: Department of Geology, Western Washington University, Bellingham, WA 98225, USA.

E-mail address: criderj@cc.wvu.edu (J.G. Crider).

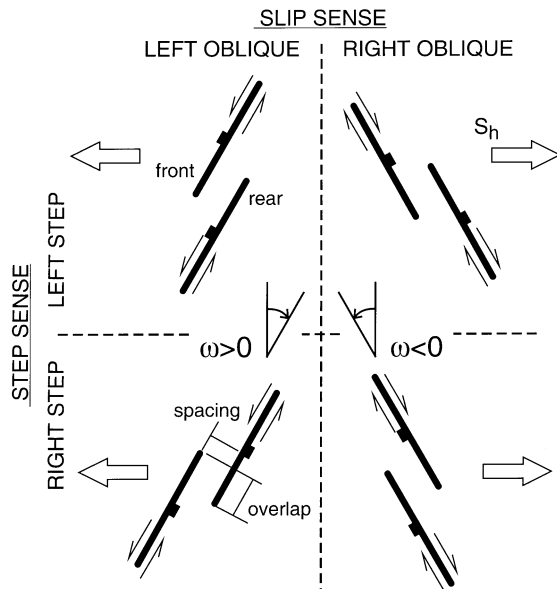


Fig. 1. The four possible combinations of step sense and oblique-slip sense. The upper row shows left-stepping fault pairs; the lower row, right-stepping pairs. The angle ω describes the deviation of the fault strike from a line perpendicular to the direction of least compressive horizontal stress (open arrows). The left column illustrates left-oblique slip and $\omega > 0$. The right column shows right-oblique slip and $\omega < 0$.

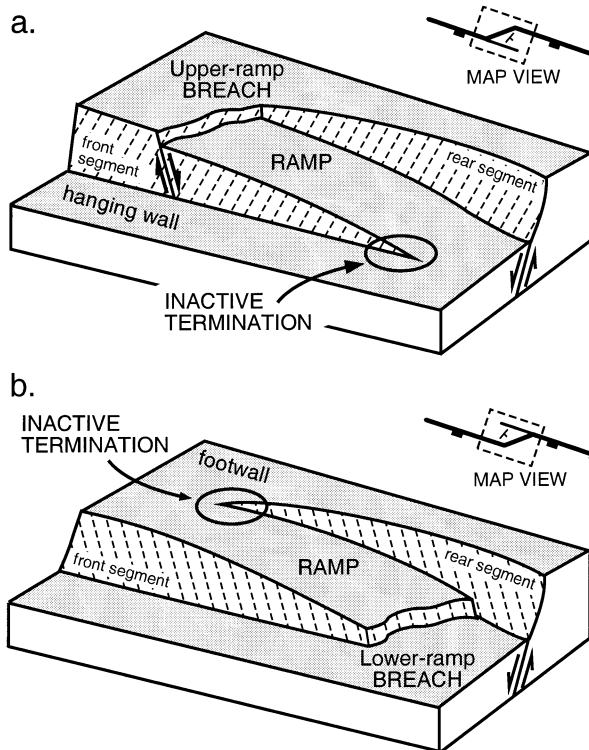


Fig. 2. Block diagrams and map views of breach geometry. (a) Upper ramp breach. Original faults are linked from the tip of the rear segment to the flank of the front segment. The ramp and an inactive fault termination are in the hanging wall of the composite structure. (b) Lower-ramp breach. Original faults are linked from the tip of the front segment to the flank of the rear segment. The ramp and an inactive fault termination are in the footwall. Insets show map view, with dashed line indicating region of block diagrams. Figures are adapted from Trudgill and Cartwright (1994).

and strain fields, and we may expect the same to be true for natural examples.

Previous work investigating the mechanics of segmented faults has focused on pure-strike slip faults (Rogers, 1980; Segall and Pollard, 1980) or pure dip-slip faults (Willemse, 1997). Whereas the mechanics that produce oblique slip on a fault have long been discussed (Williams, 1958; Bott, 1959), the consequences of fault segmentation in the context of oblique slip have not been addressed. In this contribution, I use field observations and numerical modeling to construct a mechanical rationale for zigzag fault patterns in natural and analog oblique-extension systems. Specifically, I investigate the development and location of linkage between two échelon oblique-slip faults.

This work has direct application to the interpretation of fault geometry in extensional settings. For example, many areas of active petroleum exploration, including the North Sea (Faereth et al., 1997) and the Gulf of Suez (Moustafa, 1997), are regions where extension has reactivated older structures in an oblique sense. Reactivation of basement structures has resulted in complex normal-fault patterns that play an important role in creating hydrocarbon traps and fluid migration pathways. Subsurface linking structures, such as so-called 'cross faults' connecting two échelon segments, may be below the resolution-limit of seismic data. In this case, it is impossible to determine the exact geometry of these important structures. Whether the faults are linked — and the reservoir is compartmentalized — becomes a matter of interpretation. Some workers suggest solving this problem through a simple rule of extrapolation (Pickering et al., 1997); others have attempted explicit modeling to determine the true structure (Maerten et al., 2000). Here, I present a framework for understanding how and where oblique-normal faults may link to compartmentalize a reservoir.

2. The geometry of échelon oblique normal faults

In this study, the focus is on pairs of normal faults, arranged en échelon, and striking obliquely to the direction of least-compressive horizontal stress (S_h). For the purposes of this discussion, *oblique* is any direction not parallel or perpendicular to S_h . On faults oriented obliquely to S_h , extension parallel to S_h will produce both strike slip and dip slip (Fig. 1). The oblique slip-sense distinguishes the strike-slip components: *left-oblique slip* has components of left-lateral and dip slip; *right-oblique slip* has components of right-lateral and dip slip. An acute angle of obliquity, ω , is defined to describe the deviation of fault-strike from perpendicular to S_h . For the case of orthogonal extension, $\omega = 0^\circ$. Angles of obliquity in the range of $0^\circ < \omega < 90^\circ$ produce left-oblique slip, and angles of obliquity in the range of $-90^\circ < \omega < 0^\circ$ produce right-oblique slip.

For an observer on the relay ramp facing in the dip-direction of two échelon fault segments, the fault in front of the

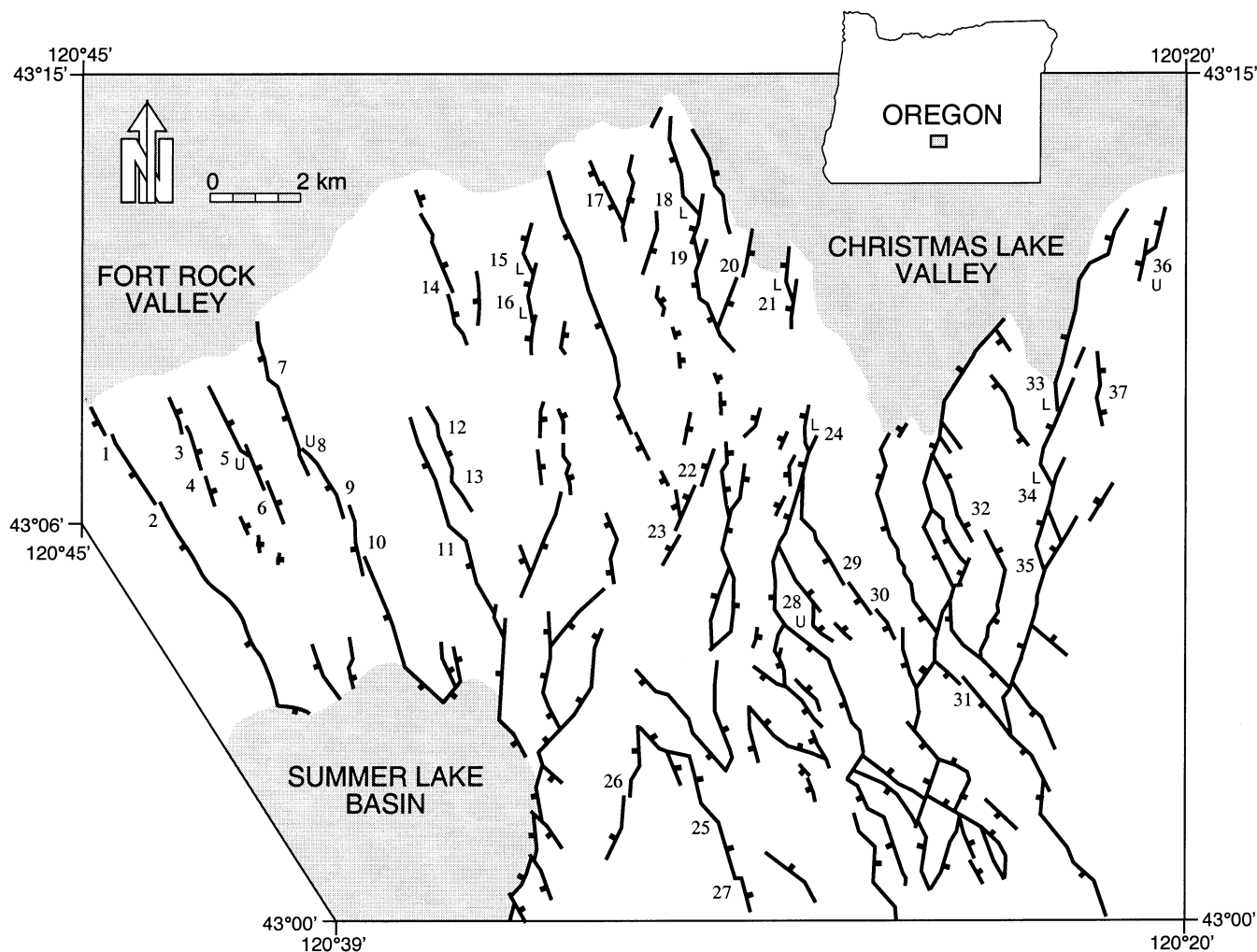


Fig. 3. Map of the fault pattern near Summer Lake, Oregon. Faults are indicated by solid lines, ticks on down-thrown side. Shaded areas are Quaternary basins. Numbers indicate fault pairs used for analysis. 'L' indicates lower-ramp breach, 'U' denotes upper-ramp breach. Other pairs do not breach the relay ramp, or the position of the breach cannot be determined. Mapped from aerial photographs (USGS NAPP series 710 ×, 1994).

observer is the *front segment* and the fault behind the observer is the *rear segment* (Figs. 1 and 2). For an observer on the trace of the rear segment, looking along strike, if the front segment is to the left, the segment pair is *left-stepping*; if the front segment is to the right, the segment pair is *right-stepping*. Thus, there are four possibilities for oblique-slip, échelon faults: left-step, left-oblique; right-step, right-oblique; left-step, right-oblique; and right-step, left-oblique. These are illustrated in Fig. 1. The dip direction changes neither the step sense nor the oblique slip-sense and thus does not create an important distinction.

The rock mass between échelon normal-fault pairs is commonly displaced into a topographic ramp (also called relay ramp or fault bridge). For the faults to link, subsequent structures must cut across, or *breach*, the ramp. Depending on the position of the linking faults, a breached ramp will become a passive feature of either the footwall or the hanging wall of the composite structure (Fig. 2). *Upper-ramp breach* indicates a secondary fault which links the two

primary faults at the topographically higher end of the ramp (equivalent to *footwall breach* of Trudgill and Cartwright (1994) and others). *Lower-ramp breach* indicates a secondary fault that links the two primary faults at the topographically lower end of the ramp (equivalent to *hanging wall breach*). These configurations may leave an *inactive termination* of one of the two primary fault segments when the breach is complete. The inactive termination is a short extension of one of the original faults that is cut-off by the breach, and therefore is not necessarily involved in continued faulting of the rock mass. We can distinguish upper-ramp from lower-ramp breaches in map view if the inactive termination is preserved. An inactive termination is left in the hanging wall of an upper-ramp breach and in the footwall of a lower-ramp breach.

We know from the study of strike slip faults that both the sense of step and the sense of slip influence fault interaction and are associated with characteristic structures in the relay zone between the faults (Rodgers, 1980; Segall and Pollard,

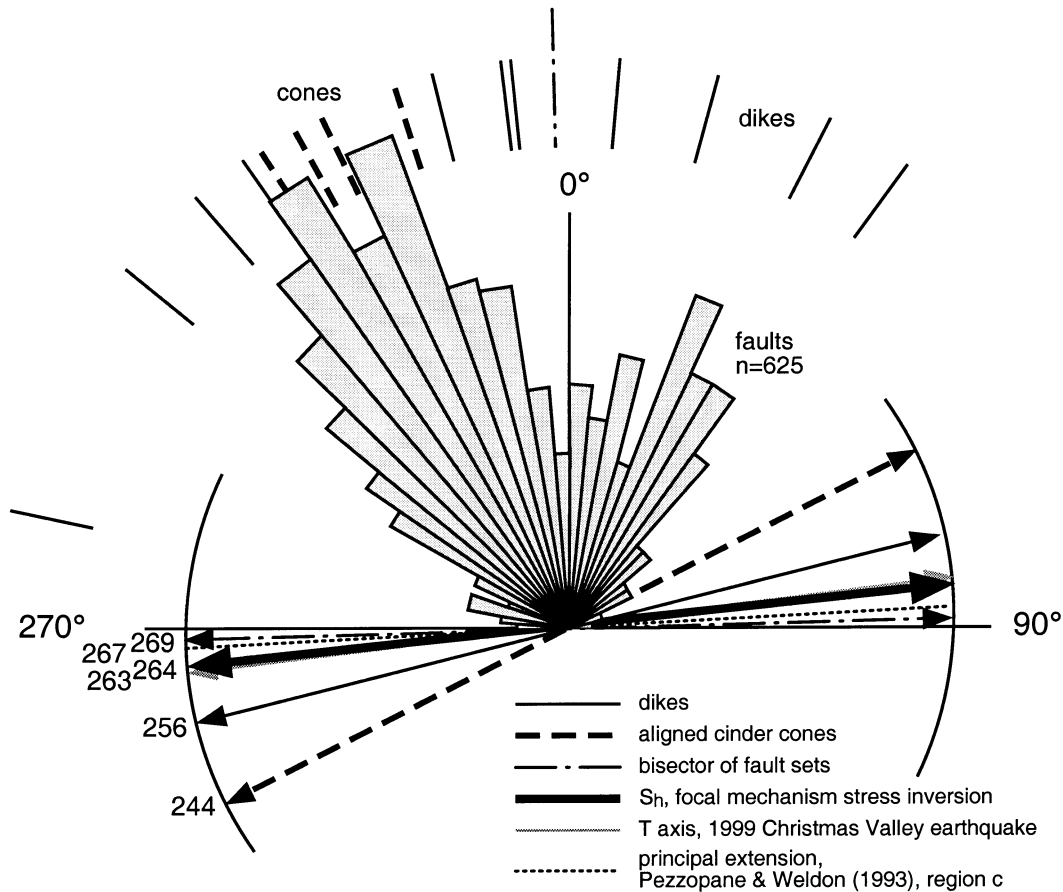


Fig. 4. Rose diagram illustrating the strike of fault scarps and other features in the study area. Fault data (Donath, 1958) are divided into 5° bins; the area of each bin is proportional to the number of scarps. Two clusters of fault strikes are evident (centered at 025° and 332°). At the perimeter of the diagram are shown the bisector of the two clusters, strikes of 11 dikes in the region, and the direction of alignments of three or more cinder cones (Walker et al., 1967). Arrows show direction of least compressive horizontal stress or regional extension. Present stress direction is determined from inversion of regional earthquake focal mechanisms and the *T*-axis of a local earthquake. Paleo-least-compressive stress is interpreted to be perpendicular to the mean strike of dikes or cone alignments. Extension direction is perpendicular to the fault bisector or inverted from earthquake moment tensors (Pezzopane and Weldon, 1993). All are compatible within uncertainty in the stress inversion (arc).

1980). For strike-slip faults on which the sense of shear and the sense of slip are different (left step, right lateral), we observe contractional structures. For strike-slip faults on which the sense of step and the sense of shear are the same (left step, left lateral), we observe extensional structures. By analogy, échelon, oblique-slip normal faults also should show characteristic secondary structures that vary with the sense of step and the sense of oblique slip.

3. Field study: Summer Lake, Oregon, USA

The case study is a region of extensional faulting in south-central Oregon at the center of Lake County, near Summer Lake and Christmas Valley (Fig. 3). The region is covered by a sequence of Tertiary volcanics, greater than 2000 m thick. The rocks are primarily basaltic and andesitic flows, with interbedded pyroclastic tuff and minor lacustrine sediments (Beaulieu, 1972; Wells, 1975). Uppermost flows in the study area have whole-rock potassium–argon ages of

6.3–6.6 ± 0.4 Ma (Diggles et al., 1990). The sub-basalt crustal structure is unknown, except at the broadest scale (Catchings and Mooney, 1988). Given the complexity of older structures to the east and west of Oregon's volcanic plateau (Ernst, 1988 and references therein), the basement structure near Summer Lake is likely to be an equally complex collage of accreted crust and multiply-deformed rocks. Thus, it is probable that the pattern of faults at Summer Lake (and elsewhere in Southern Oregon) is controlled, at least in part, by reactivation of basement structures of unknown orientation.

The tectonic setting of the region is complex. The faulting and volcanism observed may be associated with back-arc extension behind the Cascade volcanoes (Mooney and Weaver, 1989); could be the consequences of the northern termination of the broad, dextral Walker Lane shear zone (Hemphill-Haley and Weldon, 2000); and are commonly attributed to northwestern continuation of Basin-and-Range continental extension (Thompson and Burke, 1974). Despite uncertainty regarding the tectonic driving

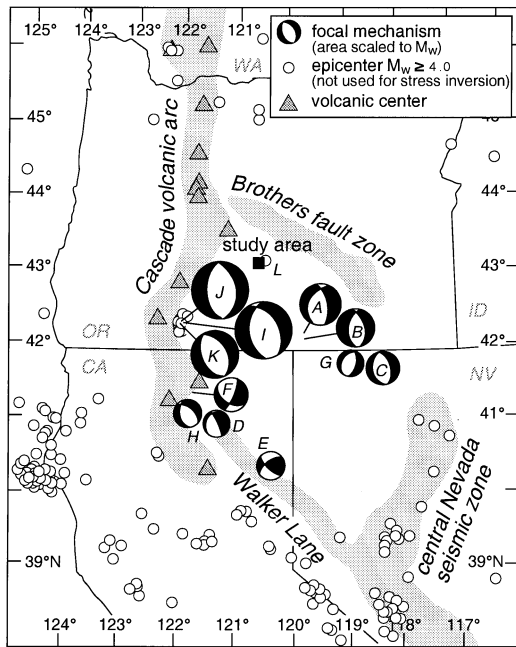


Fig. 5. Earthquake focal mechanisms used to invert for stress direction. Shaded areas represent boundaries of tectonophysiographic region used. References for focal mechanisms given in Table 1, keyed to each event by letter. Other earthquakes are from the National Earthquake Information Center (2000). Base adapted from Pezzopane and Weldon (1993).

mechanism, the study area has three characteristics important to this investigation: (1) the deformation is recent and continuing, (2) faults are clearly expressed at the surface, and (3) pairs of fault segments are observed in several configurations at different stages of interaction and linkage.

3.1. Fault pattern

In the study area, normal faults are expressed as steep topographic scarps. The faults offset the surface of late Miocene basalts and have considerable dip separation. Cosmogenic isotope analysis (using ³⁶Cl) of the present

surface of the flows indicates very low erosion rates (T. Swanson, personal communication, 1996), and so the topographic relief may appropriately reflect the total throw on the faults, after accounting for sediment-fill in the graben. Evidence for Quaternary fault activity in the study area is presented by Allison (1979), Simpson (1990) and Pezzopane and Weldon (1993). The fault pattern in this region has been previously studied by Donath (1958, 1962) and later by Reches (1978).

The region shows a complex pattern of fault scarps, clearly identifiable on topographic maps and in aerial photographs. Mappable scarps range in height from a few meters to as many as several hundred meters in height. The largest structures in the region (Winter Rim, 20 km to the southwest of the study area, and Abert Rim, 50 km to the southeast) show topographic relief of more than 750 m. The taller scarps are zigzag composites of several segments; each segment may be 100–300 m long. The composite scarps in the study area have total lengths of up to 3 km. No simple relationship between scarp height and scarp length has been identified in this study.

Map traces define four sets of faults: they strike NW–SE and dip NE or SW; or strike NE–SW and dip either NW or SE (Fig. 3). Donath (1958, 1962) identified two maxima in the strikes of fault segments near Summer Lake. On this basis he divided the faults into two conjugate sets: a primary set trending 330° and a secondary set trending 025°, separated by an angle of 55°. There is considerable scatter in these data (Fig. 4). Faults may also be classified by direction of dip, to yield the four sets recognized by Reches (1978). A greater number of scarps dip in easterly directions; however, there is greater total throw on faults that dip generally toward the west. Because dip direction is not important in this analysis, the faults are grouped into two sets (as in the Donath studies): northwest-trending and northeast-trending. From map relationships, the two sets appear to be coeval.

Pezzopane and Weldon (1993) report evidence for oblique slip on a number of Pleistocene faults near Summer Lake. In the study area, fault surfaces are not commonly

Table 1

Source parameters of earthquakes identified in Fig. 5. A–H from Patton and Zandt (1991); I–K from Braunmiller et al. (1995); L from Pacific Northwest Seismic Network (1999). L is not used for stress inversion

Event	Place name	Date (yymmdd)	Lat. N	Long. W	Mag.	Strike	Dip	Rake
A	Adel, OR	680530	42.3	119.8	5.1	001	70	– 109
B	Adel, OR	680603	42.3	119.8	5.1	176	26	– 84
C	Northwestern NV	730303	41.8	118.5	4.6	344	52	– 96
D	CA Cascades	740106	41.12	121.49	4.1	333	82	– 110
E	Northern CA	760624	40.42	120.58	4.2	131	70	148
F	CA Cascades	780801	41.45	121.88	4.6	025	79	– 38
G	Northwestern NV	800428	41.86	118.91	4.1	014	56	– 102
H	CA cascades	820621	41.16	121.94	4.2	173	58	– 54
I	Klamath Falls, OR	930921	42.32	122.03	6.0	331	47	255
J	Klamath Falls, OR	930921	42.36	122.06	6.0	351	42	269
K	Klamath Falls, OR	931204	42.29	122.01	5.5	331	48	264
L	Christmas Lake Valley, OR	990428	43.17	120.38	3.8	176	65	275

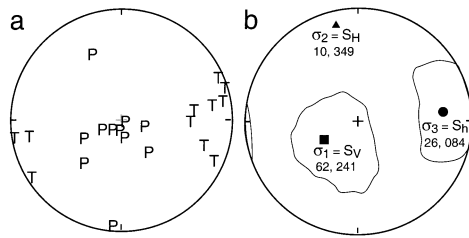


Fig. 6. Results of focal mechanism stress inversion (lower hemisphere projection). (a) *P*- and *T*-axes for the 11 focal mechanisms used in the stress inversion. (b) Best-fit stress inversion and 95% confidence regions. The least compressive stress (σ_3) is sub-horizontal and approximately E–W.

preserved, and horizontally-offset features are rare, thus there is little unambiguous evidence for strike separation along the faults. To establish the sense of oblique slip, I use independently-determined principal stress directions.

3.2. Regional principal stress directions

The regional stress directions are determined from earthquake focal mechanisms. Implicit in a regional stress inversion are the assumptions that stress in the region is spatially and temporally uniform (Gephart, 1990). Therefore, it is important to define carefully the region within which data are collected. Rather than choose an arbitrary volume around the study area, earthquakes are selected from a region delimited by major tectonic and physiographic boundaries (Fig. 5). The Brother's fault zone (Lawrence, 1974; Stewart et al., 1975) forms the northern boundary of this region, and the Cascade volcanic arc forms the western boundary. The northern Walker Lane delimits the southern edge of this deforming region. The region extends eastward up to (but not including) the central Nevada seismic zone (Doser, 1986). These four features trace a rough parallelogram. The Summer Lake study area falls into the northwest quadrant of this area.

Fig. 5 shows the distribution of seismic events in southern Oregon and vicinity in the past 90 years with moment magnitude (M_w) greater than 4.0, and for which there are published focal mechanisms. Twenty-three events of $M_w > 4.0$ are recorded in the region delimited by the boundaries described above. To avoid the complications of locally-triggered aftershock events, only the largest shocks of the 1993 Klamath Falls sequence are included, leaving eleven events (A–K, Fig. 5 and Table 1). Focal mechanisms taken from published sources (Table 1) were used to invert for the stress directions, following the method of Gephart (1990, also Gephart and Forsyth, 1984). Each event was given equal weight. The solution yields a stress tensor with the least compressive stress sub-horizontal ($S_h = \sigma_3$) and oriented E–W or slightly ENE–WSW (Fig. 6). The greatest compressive stress is near vertical ($S_v = \sigma_1$) and the intermediate stress is approximately N–S ($S_H = \sigma_2$). This result is somewhat more westerly than the NW–SE extension commonly attributed to much of the Basin and

Range (Zoback and Zoback, 1989). To check that the regional stress inversion is appropriate for the study area, I compare the results with a local event not used in the inversion. The azimuth of S_h determined from the regional stress inversion (264) is almost identical to the azimuth of the *T*-axis (263) of the focal mechanism for a small earthquake (magnitude 3.8) in the study area (L in Table 1).

Paleostress analysis of structures from the study area supports an ENE–WSW orientation for S_h , indicating that this direction may have persisted for longer than the past century. Late Miocene–Pliocene dikes in the vicinity of the study area have a range of orientations similar to the faults (Walker et al., 1967; Fig. 4). A line perpendicular to the mean strike of the dikes runs ENE–WSW. Alignments of three or more cinder cones north of the study area (mapped by Walker et al. (1967) as late Miocene to Recent in age) trend NW (Fig. 4). The alignments of cones can be interpreted to be the result of ENE–WSW least compressive stress. Allison (1979) reports N–S alignment of joints in lacustrine sediments of the Fort Rock Valley, requiring (at least local) E–W effective tension. The dikes, cones and joints yield directions for S_h that are consistent within the error of the focal mechanism stress inversion (Fig. 4). None of these observations alone is conclusive, but together they lend credence to persistence of the principal stress directions from Neogene to present.

Analysis of the strain tensor in the region compares favorably. For an orthorhombic fault pattern as seen at Summer Lake, the direction of maximum extension is perpendicular to the bisector of the angle between the two fault sets (Reches 1978). This falls E–W (Fig. 4). Pezzopane and Weldon (1993) (and Fig. 4) sum the slip vectors from earthquake moment tensors to determine the extension direction in a similar region (their region c), and they obtain similar results.

The seismic record and geologic record show that the region is extending E–W or slightly ENE–WNW in response to a similarly oriented minimum horizontal stress (S_h). Both fault sets are oriented obliquely to this direction. Thus, NE-striking faults resolve left-oblique slip and NW-striking faults resolve right-oblique slip.

3.3. Fault linkage

A principal mechanism for fault growth in the region appears to be the linkage of small fault segments into composite structures. Short fault segments with relatively small amounts of throw (for example, pairs 3 and 4, Fig. 3) are commonly arranged en échelon. Segments with intermediate length and throw (pairs 8 and 9) show segment interaction and breaching of the relay ramps between them. The fault segments with the greatest throw (pairs 34 and 35) are linked to form larger, through-going scarps with zigzag traces. The correlation between fault-trace geometry and progression in length and throw suggests an evolution

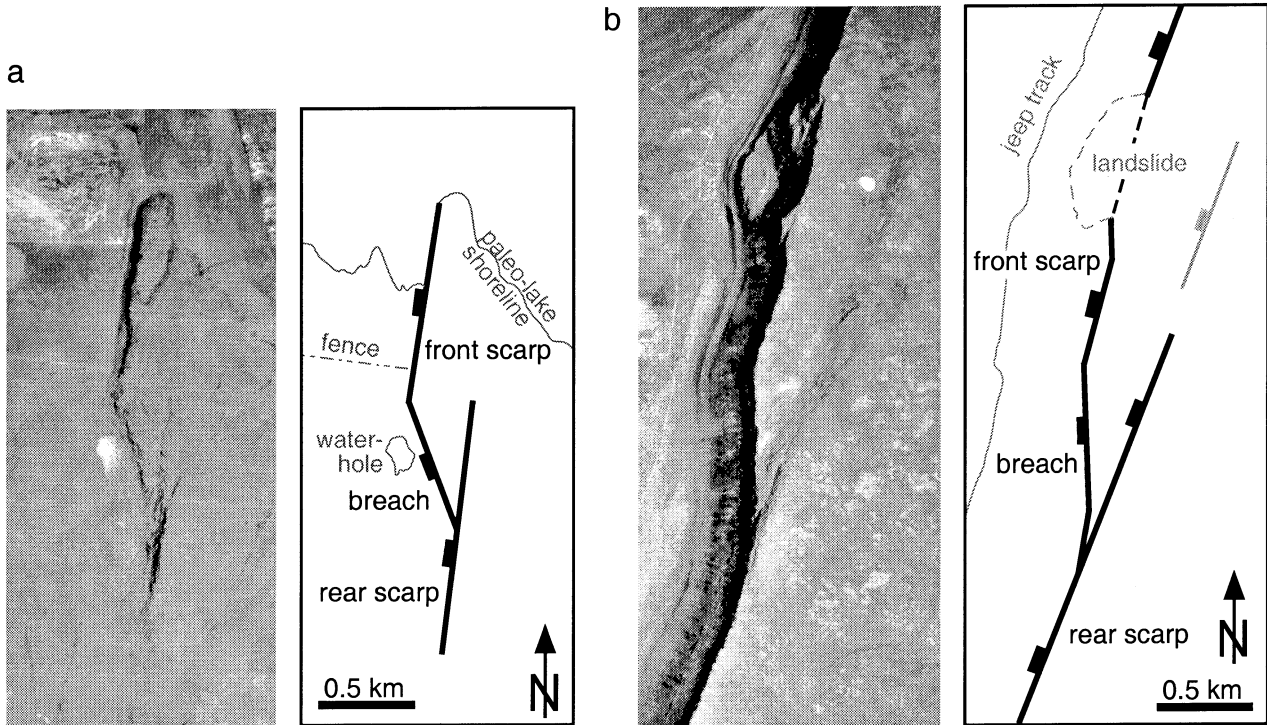


Fig. 7. Two examples of lower-ramp breaches from the study area (vertical aerial photographs and interpretation). (a) Fault pair 21 from Fig. 3 (photo excerpted from USGS NAPP 7101-114). The front and rear scarps each have a maximum height of about 60 m; the breaching scarp is about 20 m high. An inactive termination can be identified in the footwall of the front scarp, helping to define a rubbly ramp that is breached at the bottom. (b) Fault pair 33 from Fig. 3 (photo excerpted from USGS NAPP 7101-42). The faults are part of Burma Rim, a well-developed zigzag scarp at the eastern edge of the study area. The front scarp, breach, and rear scarp are in excess of 150 m high. The inactive termination of the rear scarp (in the footwall of the front scarp) is about 10 m high, indicating that the structure was breached at an early stage.

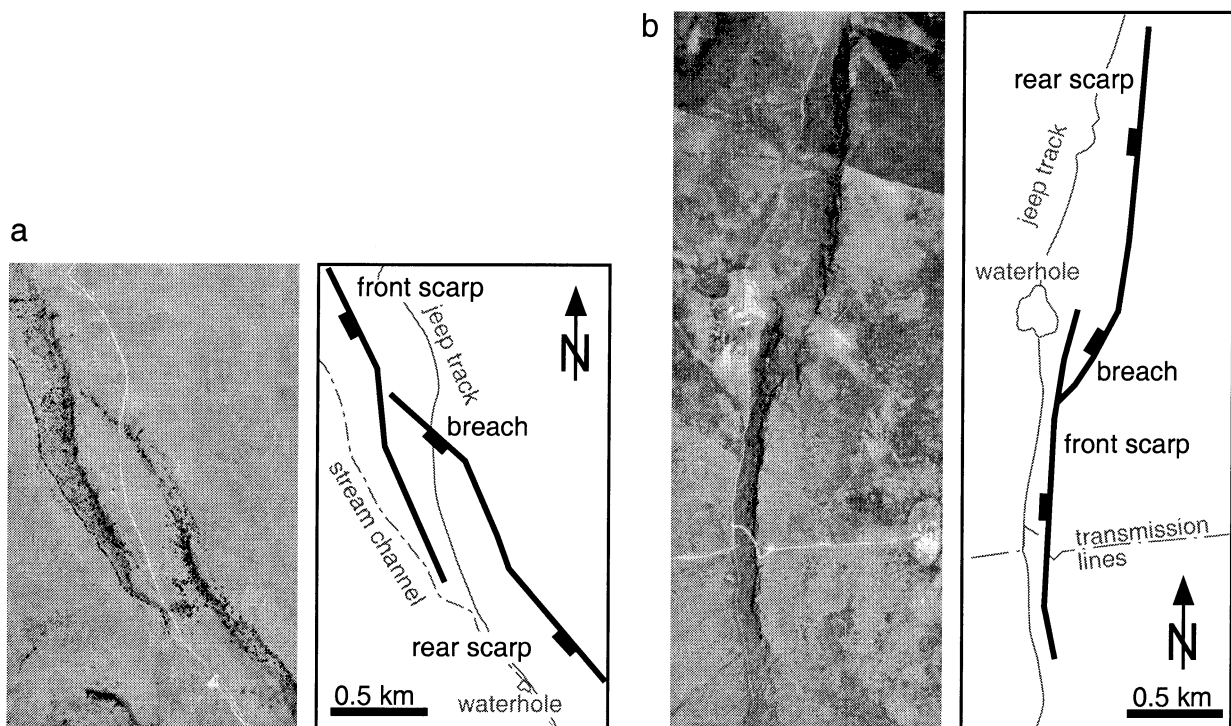


Fig. 8. Two examples of upper-ramp breaches from the study area. (a) Fault pair 8 from Fig. 3 (photo is excerpted from USGS NAPP 7101-235). The front scarp has a maximum height of 87 m and the rear scarp is 66 m high. The breach cuts across the top of a well-defined ramp and varies in height from about 10 m near the rear scarp to less than 1 m near the front scarp. (b) Fault pair 36 from Fig. 3 (photo excerpted from USGS NAPP 7100-120). The front and rear scarps are both approximately 60 m high. An inactive termination of the front scarp is visible in the hanging wall of the rear scarp.

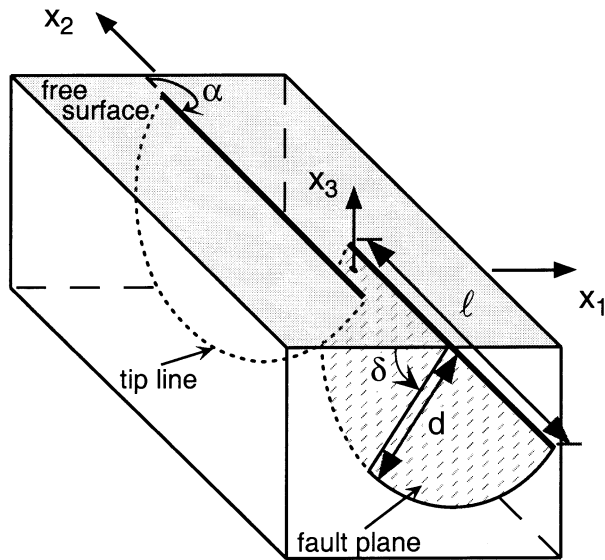


Fig. 9. Geometric elements of the model configuration. Global coordinates originate at the center of the relay and on the free surface of the half space. x_1 , x_2 define a horizontal plane, x_3 is vertical. Modeled faults have semi-elliptical tip lines with one axis coincident with the free surface. The dimensions of the faults are described as the trace length (l) and the down-dip length (d). The orientation of the modeled faults is described by the azimuth of the faults (α), measured clockwise from the x_2 axis, and the fault dip (δ), measured from the free surface.

from échelon segments to partially-linked segments to composite faults (see also Cartwright et al., 1995).

In order to link, the faults must breach the relay ramp between them, and this commonly happens in one of two ways (Trudgill and Cartwright, 1994). The rear segment connects to the flank of the front segment, thus breaching the upper ramp and leaving an inactive termination in the hanging wall (Fig. 2a). Alternatively, the front segment connects to the flank of the rear segment, breaching the lower ramp, and leaving an inactive tip in the footwall (Fig. 2b). The scarp of the inactive termination may become eroded or buried during subsequent development of the normal fault system.

Because these structures are ephemeral on a geologic time scale, we catch few pairs in the act of breaching. In the study area, 37 pairs of échelon segments were examined, identified by number in Fig. 3. The characteristics of the selected pairs are as follows: (1) they are clearly identifiable in aerial photographs (USGS NAPP series 710 ×, 1994); (2) the segments in each of these pairs are sub-parallel and of similar length; (3) the two segments may overlap or underlap; (4) they are spaced (perpendicular to strike) by a distance not greater than their individual trace lengths; (5) no additional segments intersect the pair in the vicinity of the relay zone; and (6) the scarps are not influenced by lateral changes in lithology or significant geomorphic disturbance. Other fault pairs and segment boundaries exist in the study area but do not meet these criteria and were therefore omitted.

A fault pair was determined to be breached if a fault scarp

connecting the two segments was visible in aerial photographs. Seventeen of the 37 selected pairs are soft-linked: there is a ramp between them, but no breach is visible at the surface. Nine fault pairs are connected, but the geometry of the breach cannot be determined confidently. The remaining 11 pairs preserve the relay-breaching structures. Seven of these pairs, marked with an 'L' in Fig. 3, are breached at the lower-ramp, as determined by the presence of an inactive termination in the footwall of the structure. Two of these structures (numbers 21 and 33) are illustrated in Fig. 7. Four pairs, marked with a 'U', show inactive terminations in the hanging wall, and thus may be identified as upper-ramp breaches. Two examples (numbers 8 and 36) are shown in Fig. 8.

Further examination of the breached ramps reveals an interesting pattern. For the NE-striking pairs of fault segments (across which left-oblique slip is resolved) there are seven left-stepping pairs. All seven show inactive terminations in the footwall and thus are lower-ramp breaches. The remaining left-oblique pair (36) is right-stepping and has an inactive termination in the hanging wall: it is an upper ramp breach. For three NW-striking pairs of fault segments (across which right-oblique slip is resolved), two are left-stepping pairs (5 and 8) and one is a right-stepping pair (28). All three are breached in the upper ramp. Thus, 10 of the 11 linking structures can be described as follows: those with the same slip sense and step sense (e.g. left-oblique, left stepping) are lower ramp breaches; those with opposite slip sense and step sense (e.g. right-oblique, left stepping) have upper ramp breaches. The predominance of this pattern strongly suggests a causal link between step sense, oblique-slip sense and the position of relay-breaching structures.

4. Geomechanical modeling

Numerical models of échelon fault segments are employed to find a geomechanical explanation for this phenomenon. To model oblique-slip faults, I use *Poly3D*, a three-dimensional, boundary-element-method, numerical code (Thomas, 1993). The code has been benchmarked and shown to reproduce analytical solutions to within a few percent (Crider and Pollard, 1998). The faults are idealized as semi-elliptical surfaces in a homogeneous elastic half-space (Fig. 9). The material is assigned a Poisson ratio of 0.25, a shear modulus of 30 GPa, and a density of, $\rho = 2820 \text{ kg m}^{-3}$, approximating basalt (Birch, 1966).

The geometry of the model is shown in Fig. 9. Both faults have the same dimensions: they are 2 km long where they break the free surface and 1 km tall at the center. They have parallel strike, and they dip 60° in the same direction. The strike of the faults is given by α , clockwise from x_2 and is varied among trials to produce oblique slip. The faults overlap 500 m at the surface and are spaced 300 m perpendicular to strike. The pair is left-stepping for all trials. There is no

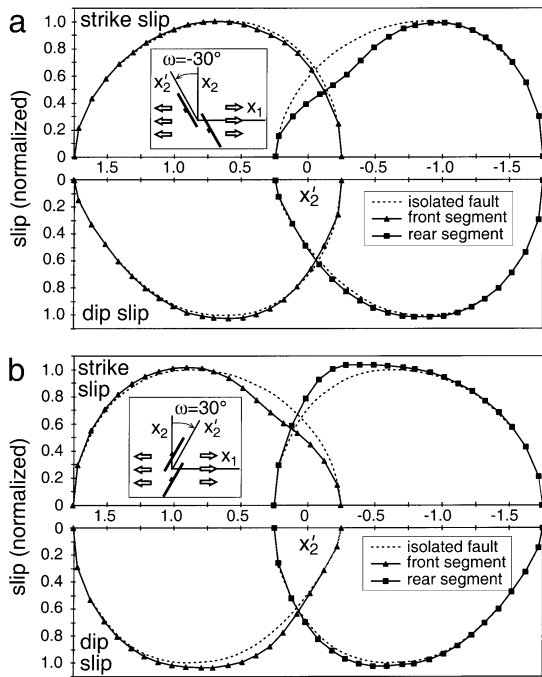


Fig. 10. Strike and dip slip distribution on interacting oblique-slip normal faults. Slip is measured at the free surface of the modeled half-space. Values are normalized to the maximum slip of an isolated oblique-slip fault. The top portion of each plot shows strike slip, the bottom, dip slip. x'_2 is the coordinate parallel to the strike of the faults, and $x'_2 = 0$ at the center of the overlap region. Insets show model configuration. (a) Fault pair, $\omega = -30^\circ$, with opposite sense of step and sense of oblique slip (upper-ramp breach). (b) Fault pair, $\omega = +30^\circ$, with the same sense of step and slip (lower-ramp breach).

friction on the faults. Lack of friction is not realistic, but it allows us to observe one end-member of fault behavior: the maximum possible slip and maximum fault interaction.

The model is subject to an isotropic lithostatic load, L , that increases linearly downward according to $L = -\rho g x_3$. Deformation is driven by a uniaxial remote tension, $-T$, acting parallel to x_1 . This condition effectively reduces the confining stress in x_1 , such that $\sigma_3 = S_h = L - T$, $\sigma_2 = S_H = L$ and $\sigma_1 = S_v = L$. If x_2 is ‘north’, then the least compressive principal stress (S_h) is ‘east–west’. For details regarding the implementation of these boundary conditions in *Poly3D*, please refer to Crider and Pollard (1998).

The numerical code calculates the distribution of slip across the faults and stresses induced in the material by slip-related deformation, including bending of the ramp between the faults. The maximum Coulomb shear stress (S_C) is calculated from the principal stresses (Jaeger and Cook, 1979):

$$S_C = \left(\frac{(\sigma_1 - \sigma_3)}{2} \right) \sqrt{1 + \mu^2} + \mu \left(\frac{(\sigma_1 + \sigma_3)}{2} \right), \quad (1)$$

where $\mu = 0.6$ is the coefficient of internal friction. S_C describes the relationship between shear and normal traction on optimally-oriented planes of possible shear failure. S_C is

used to evaluate the propensity of those surfaces to slip and form new secondary faults. Normalized to its remote value, S_C is a measure of the stress perturbation around the faults.

The slip distributions and change in Coulomb stress were evaluated for pairs of semi-circular faults that have been rotated $\omega = \pm 30^\circ$ with respect to x_2 . The arrangement of the faults with respect to each other and the remaining boundary conditions do not differ from trial to trial. If the fault pair is oblique to S_h , a significant component of strike slip is introduced (Fig. 10). The magnitude of the strike-slip displacement in both cases ($\omega = \pm 30^\circ$) is the same order as the magnitude of the down-dip displacement, but the sense of strike slip (right-lateral or left-lateral) correlates with the sign of ω .

The distribution of slip is asymmetrical on oblique slip faults, and the sense of asymmetry changes with the sense of slip. Fig. 10a shows the distribution of dip slip and of strike slip at the free surface on a fault pair with opposite sense of step and oblique slip (left-stepping, right-oblique). By comparison with the slip distribution on an isolated right-oblique fault (dashed line), it is evident that fault interaction has had little effect on the dip component of slip on either fault. The dip slip on both the front and rear segments is slightly enhanced (1–2%) just outside the relay zone ($0.75 > x'_2 > 0.25$ and $-0.25 > x'_2 > -0.75$), and dip slip on the front segment is slightly diminished (~1%) within the relay zone ($0.25 > x'_2 > -0.25$). On the front segment, strike slip is diminished slightly (1–2%) from the center of the fault through the relay zone. The strike component of slip on the rear segment is affected more profoundly: the strike component of slip on this segment is reduced as much as 20%, especially in the vicinity of the front-segment termination.

Fig. 10b shows the distribution of slip on a fault pair with the same sense of step and oblique slip (left-stepping, left-oblique). Dip slip on both faults is enhanced 2–3% on the rear segment and nearly 10% on the front segment, especially between the centers of the segments and the relay zone. On the rear segment, strike slip is increased by as much as 15% relative to an isolated fault. On the front segment, strike slip is diminished by about the same percentage. These effects are greatest in the vicinity of the other segment termination ($x'_2 = \pm 0.25$).

Three-dimensional analysis has shown that the fault interaction is greatest where tiplines are closest (Crider and Pollard, 1998). Horizontal slices through the models at a depth of 660 m show the greatest stress perturbation and illustrate the influence of oblique slip on secondary deformation in the relay zone. Fig. 11 illustrates the changing stress distribution with increasing obliquity in both positive and negative ω . The contours show the distribution of maximum Coulomb shear stress normalized to its remote value.

In the orthogonally loaded case ($\omega = 0^\circ$) there is an asymmetry between the footwall and hanging wall of the faults, such that in the footwall (at this depth) the maximum

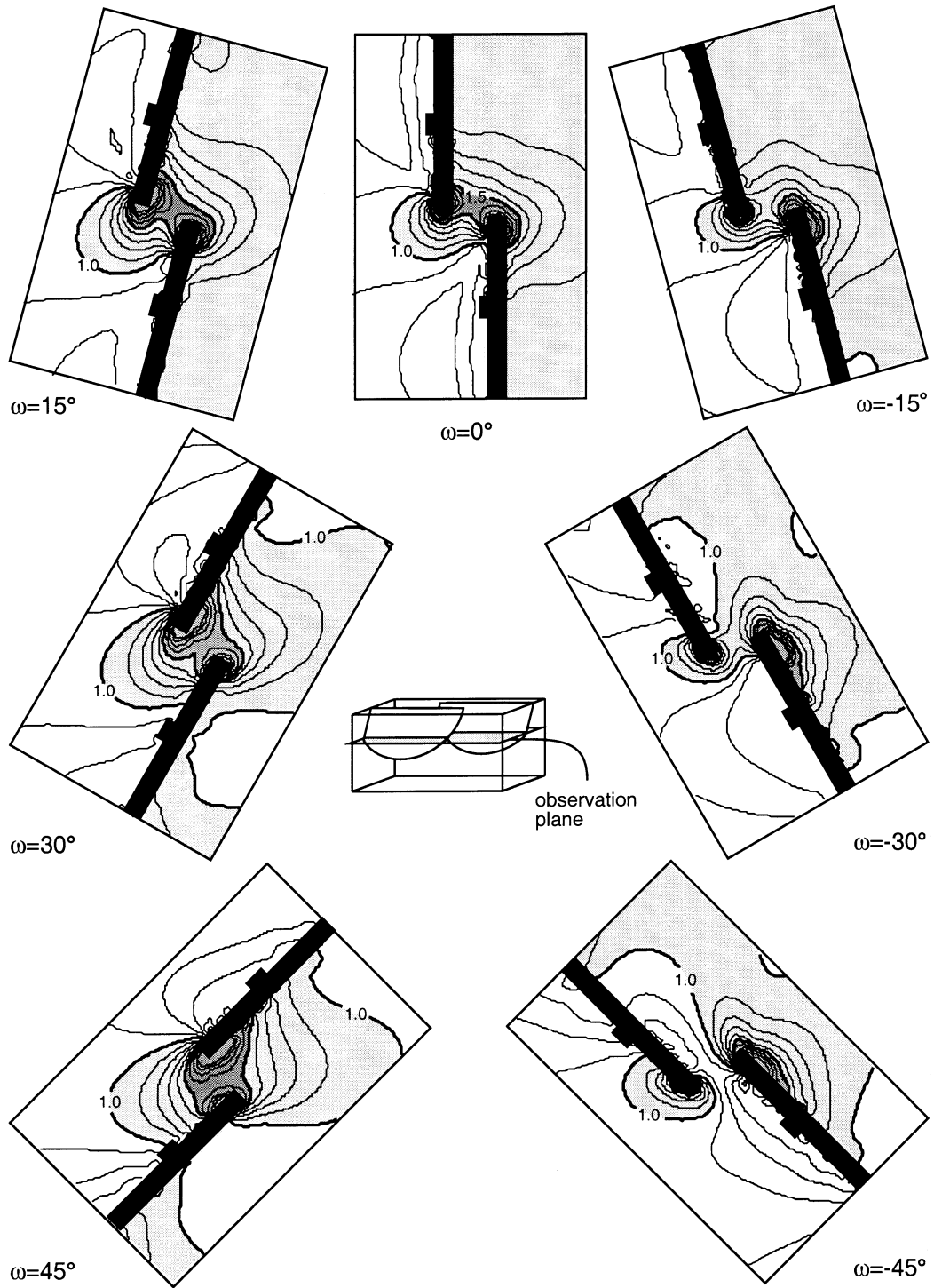


Fig. 11. Contours of normalized S_C for fault pairs with increasing angles of obliquity (ω) relative to the direction of least compressive stress (parallel to the top of the page). Shading indicates region with S_C greater than remote value. Horizontal slices are taken through the models at a depth of $x_3 = 660$ m, where the fault tip-lines are closest. Black bars indicate trace of the faults at that depth in the model, tics on down-thrown side. Top center: $\omega = 0^\circ$, fault pair under orthogonal extension. Left side: $\omega > 0$, fault pair with same step sense and oblique-slip sense. Right side: $\omega < 0$, fault pairs with opposite step and oblique-slip.

Coulomb shear stress is everywhere greater than the remote value. In the hanging wall, S_C is reduced except in the vicinity of the relay zone. In the region of fault overlap, the effect of fault interaction is clearly visible: S_C in the relay

zone is 150% of the remote value. Near the two fault tips, the stress increase is approximately the same magnitude; due to the footwall–hanging wall asymmetry, secondary deformation is favored somewhat in the footwall and

ahead of the rear segment, in the upper part of the relay ramp.

For the oblique slip cases, the importance of the footwall–hanging wall asymmetry decreases, because a portion of the strain is taken up by strike slip. The region of S_C -increase in the footwall shrinks correspondingly. The asymmetry in the stress distribution near the fault tips increases; thus the magnitude of the stress perturbation in the relay zone is strongly influenced by the sense of oblique slip.

For trials in which the sense of step is opposite to the sense of oblique-normal slip (right side of Fig. 11), the strike-slip component on the faults produces a compressive (restraining) step, and the region of S_C -increase is diminished relative to the orthogonally-loaded case. In the relay zone, the magnitude of S_C progressively decreases with increasing obliquity, until the stress is reduced relative to the remote value. The distribution of stress is also different from the orthogonally-loaded case. The stress perturbation in the vicinity of the rear-segment tip line is the primary feature of these patterns, whereas other stress increases are confined to the very-near-tip region of the front segment. This stress distribution indicates a greater potential for faulting around the tip of the rear segment and potential abandonment of the tip of the front segment. Although secondary deformation is less likely due to reduced stress overall, if the relay is breached under this loading configuration, an upper-ramp breach is favored, with the breach connecting the tip of the rear segment to the flank of the front segment.

In the second set of oblique trials (left side of Fig. 11), the sense of step is the same as the sense of oblique-normal slip. In these trials, the strike component of slip produces a tensile (releasing) step, elevating the Coulomb stress in the relay zone and enhancing the likelihood of relay-breaching structures. The zone of increased Coulomb stress is broader than in the opposite step/slip trials, but the magnitude at the center of the relay is not greater than that for the orthogonally-extended case (150% of the remote value). The zone of increased stress continues into the footwall of both faults and, unlike the other examples, into the hanging wall of the rear segment. The asymmetry of the stress distribution is opposite to that of the first set of trials. The greatest stress increases are broad in the vicinity of the front-segment tip but are constrained to the near-tip field of the rear segment. Under this loading configuration, the greatest potential for deformation is ahead of the front-segment tip in the hanging wall of the rear segment, at the lower part of the relay ramp. Thus, configurations with the same sense of step and slip favor a lower-ramp breach.

5. Conclusions

This study brings together two sets of independent observations — field and numerical — that suggest the same

relationship between oblique-slip, sense of step, and the structures linking échelon normal faults. Échelon fault-segments with the same sense of step and oblique slip are likely to breach in the lower part of their relay ramp. Échelon fault-segments with opposite sense of step and oblique slip are likely to breach in the upper ramp.

In the study area, all of the pairs with opposite sense of step and oblique slip for which the position of the breach could be confidently determined (three out of three) adhere to this relationship and are breached in the upper ramp. Most of the pairs with the same sense of step and oblique slip (seven out of eight) show lower-ramp breaches and, thus, also conform. These observations are bolstered by published accounts of oblique slip on normal fault pairs, both natural and analog. Bonini et al. (1997) show a left-stepping, left-oblique échelon fault pair with a lower-ramp breach in their map of faults in the Lagano Lake region of the Main Ethiopian Rift (their fig. 3b). Linked fault segments in the North Sea mapped by Faerseth et al. (1997) display this relationship, with few exceptions. Richard (1991) shows a left-stepping, right-oblique, upper-ramp breach in an analog model of faults growing over a reactivated basement fault (his fig. 4a). The clay-over-latex analog experiments of oblique rifting of Clifton et al. (2000) show numerous examples that correspond to this pattern (their fig. 3).

In their analog study, Higgins and Harris (1997) describe the development of an upper-ramp breach linking a right-stepping, left-oblique fault pair (faults 3 and 4 in their fig. 5). The segments are initially separate. With increasing extension, the tip of the rear segment propagates across the top of the ramp and links to the flank of the front segment. The termination of the front segment is then abandoned, as the composite fault — now with a zigzag trace — accommodates further extension. This is the scenario anticipated by the models and field observations presented here.

Changes in fault height or overlap will influence the magnitude of stress perturbation in the relay zone, but the effect of changing these geometric parameters does not change the anticipated map-pattern of linkage (Crider and Pollard, 1998). The model results presented here indicate that altering the strike of the faults relative to the direction of applied load *will* alter the geometry of linkage, because the symmetry of the system is changed. Oblique slip (and the sense of obliquity) has an impact on both the magnitude and the shape of the regions of stress concentration around échelon faults. The stress perturbation favors faulting of the upper-ramp and abandonment of the tip of the front segment of an échelon pair for pure-dip slip and for oblique slip that produces a restraining step. The stress perturbation favors fracturing the lower-ramp and abandoning the tip of the rear segment for oblique slip that produces a releasing step.

This study does not address the origin of oblique-slip faults or of échelon arrays of normal faults. The purpose here was to address the *consequences* of oblique slip on further development of a normal fault system. Oblique-slip

faults may be the product of deformation above reactivated basement structures (as is likely in the study area), or they may be controlled by a pre-existing structural fabric. Analog experiments produce échelon arrays with opposite step and slip sense, almost exclusively (Richard, 1991; Smith and Durney, 1992; Higgins and Harris, 1997). In natural fault systems, both types of arrays are observed (Cartwright et al., 1995; Bonini et al., 1997; this study).

Oblique slip and the échelon arrangement of fault segments influence slip distribution across faults and stress perturbation around faults. These, in turn, influence fault growth and the geometry of fault linkage. The position of relay-breaching structures may provide a tool for the identification of oblique slip and the evaluation of regional stress directions. Moreover, understanding why and where échelon fault pairs are breached may allow us to predict the position of fault linkage in the sub-surface where these structures cannot be observed or imaged directly.

Acknowledgements

This work was supported by National Science Foundation grant EAR-9725372. The author gratefully acknowledges the contribution of D.D. Pollard to the development of ideas presented here. The manuscript benefited from discussions with R.A. Harris, E. Koenig, S.A. Kattenhorn, B.D. Trudgill and E.J. Steig, from thoughtful reviews by J.A. Cartwright and T.G. Blenkinsop, and from an exceptionally careful reading by S.K. Pezzopane.

References

- Allison, I.S., 1979. Pluvial Fort Rock Lake, Lake County, Oregon. Oregon Department of Geology and Mineral Industries. Special Paper, 7.
- Baldrige, W.S., Ferguson, J.F., Braile, L.W., Wang, B., Eckhardt, K., Evans, D., Schultz, C., Gilpin, B., Jiracek, G.R., Biehler, S., 1994. The western margin of the Rio Grande Rift in northern New Mexico; an aborted boundary?. *Geological Society of America Bulletin* 106, 1538–1551.
- Bartholomew, I.D., Peters, J.M., Powell, C.M., 1992. Regional structural evolution of the North Sea; oblique slip and the reactivation of basement lineaments. In: Parker, J.R. (Ed.). *Petroleum Geology of Northwest Europe; 4th Conference*. , pp. 1109–1122.
- Beaulieu, J.D., 1972. Geologic formations of eastern Oregon. Oregon Department of Geology and Mineral Industries Bulletin, 72.
- Birch, F., 1966. Compressibility and elastic constants. In: Clark Jr, S.P. (Ed.). *Handbook of Physical Constants*. Geological Society of America Memoir 97, pp. 223–290.
- Bonini, M., Souriot, T., Boccaletti, M., Brun, J.P., 1997. Successive orthogonal and oblique extension episodes in a rift zone: Laboratory experiments with application to the Ethiopian Rift. *Tectonics* 16, 347–362.
- Bott, M.H.P., 1959. The mechanics of oblique slip faulting. *Geological Magazine* XCVI, 109–117.
- Braunmiller, J., Nábèlek, J., Leitner, B., Qamar, A., 1995. The 1993 Klamath Falls, Oregon, earthquake sequence: source mechanisms from regional data. *Geophysical Research Letters* 22, pp. 105–108.
- Cartwright, J.A., Trudgill, B.D., Mansfield, C.S., 1995. Fault growth by segment linkage; an explanation for scatter in maximum displacement and trace length data from the Canyonlands Grabens of SE Utah. *Journal of Structural Geology* 17, 1319–1326.
- Caskey, S.J., Wesnousky, S.G., Zhang, P., Slemmons, D.B., 1996. Surface faulting of the 1954 Fairview Peak (MS 7.2) and Dixie Valley (MS 6.8) earthquakes, central Nevada. *Bulletin of the Seismological Society of America* 86, 761–787.
- Catchings, R.D., Mooney, W.D., 1988. Crustal structure of east central Oregon; relation between Newberry Volcano and regional crustal structure. *Journal of Geophysical Research* 93, 10,081–10,094.
- Chapin, C.E., Cather, S.M., 1994. Tectonic setting of the axial basins of the northern and central Rio Grande Rift. *Geological Society of America Special Paper* 291, 5–25.
- Chorowicz, J., Sorlien, C., 1992. Oblique extensional tectonics in the Malawi Rift, Africa. *Geological Society of America Bulletin* 104, 1015–1023 (with Suppl. Data 92-23).
- Clifton, A.E., Schlische, R.W., Withjack, M.O., Ackermann, R.V., 2000. Influence of rift obliquity on fault-population systematics; results of experimental clay models. *Journal of Structural Geology* 22, 1491–1509.
- Crider, J.G., Pollard, D.D., 1998. Fault linkage: three-dimensional mechanical interaction between echelon normal faults. *Journal of Geophysical Research* 103, 24,373–24,391.
- Diggles, M.F., Conrad, J.E., Soreghan, G.A., 1990. Geologic map of the Diablo Mountain Wilderness Study Area, Oregon. U.S. Geological Survey Map MF-2121, scale 1:48,000.
- Donath, F.A., 1958. Basin and Range structure of south-central Oregon. Ph.D. thesis, Stanford University.
- Donath, F.A., 1962. Analysis of Basin and Range structure. *Geological Society of America Bulletin* 71, 1–15.
- Doser, D.I., 1986. Earthquake Processes in the Rainbow Mountain–Fairview Peak–Dixie Valley, Nevada, Region, 1954–1959. *Journal of Geophysical Research* 91, 12,572–12,586.
- Ernst, W.G. (Ed.), 1988. *Metamorphism and Crustal Evolution of the Western United States*. Prentice Hall, Englewood Cliffs, NJ.
- Faersth, R.B., Knudsen, B.E., Liljedahl, T., Midboe, P.S., Soderstrom, B., 1997. Oblique rifting and sequential faulting in the Jurassic development of the northern North Sea. *Journal of Structural Geology* 19, 1285–1302.
- Freund, R., Merzer, A.M., 1976. The formation of rift valleys and their zigzag fault patterns. *Geological Magazine* 113, 561–568.
- Fridrich, C.J., Whitney, J.W., Hudson, M.R., Crowe, B.M., 1999. Space-time patterns of late Cenozoic extension, vertical axis rotation, and volcanism in the Crater Flat basin, Southwest Nevada. *Geological Society of America Special Paper* 333, 197–212.
- Gephart, J.W., 1990. Stress and the direction of slip on fault planes. *Tectonics* 9, 845–858.
- Gephart, J.W., Forsyth, D.W., 1984. An improved method for determining the regional stress tensor using earthquake focal mechanism data: application to the San Fernando earthquake sequence. *Journal of Geophysical Research* 89, 9305–9320.
- Hemphill-Haley, M.A., Weldon, R.J., 2000. Role of faulting and volcanism in strain accommodation within the Oregon Basin and Range. *Geological Society of America Abstracts with Programs* 32, 337.
- Higgins, R.I., Harris, L.B., 1997. The effect of cover composition on extensional faulting above re-activated basement faults; results from analog modeling. *Journal of Structural Geology* 19, 89–98.
- Jaeger, J.C., Cook, N.G.W., 1979. *Fundamentals of Rock Mechanics*. Chapman and Hall, London.
- Lawrence, R.D., 1974. Northern termination of the Basin and Range Province in Oregon. *Proceedings of the Oregon Academy of Sciences* 10, 68–69.
- Maerten, L., Pollard, D.D., Karpuz, R., 2000. How to constrain 3D fault continuity and linkage using reflection seismic data: a geomechanical approach. *American Association of Petroleum Geologists Bulletin* 84, 1311–1324.
- Mooney, W.D., Weaver, C.S., 1989. Regional crustal structure and

- tectonics of the Pacific coastal states California, Oregon, and Washington. *Geological Society of America Memoir* 172, 129–161.
- Moustafa, A.R., 1997. Controls on the development and evolution of transfer zones; the influence of basement structure and sedimentary thickness in the Suez Rift and Red Sea. *Journal of Structural Geology* 19, 755–768.
- National Earthquake Information Center, 2000. Earthquake Data Base. U.S. Geological Survey. <http://neic.usgs.gov/neis/epic/database.html>.
- Oudmayer, B.C., de Jager, J., 1992. Fault reactivation and oblique-slip in the southern North Sea. In: Parker, J.R. (Ed.), *Petroleum Geology of Northwest Europe*, 4th Conference. pp. 1281–1290.
- Pacific Northwest Seismic Network, 1999. Data file 99042808061o. University of Washington. http://www.geophys.washington.edu/SEIS/EQ_Special/WEBDIR_99042808061o/welcome.html.
- Patton, H.J., Zandt, G., 1991. Seismic moment tensors of Western U.S. earthquakes and implications for the tectonic stress field. *Journal of Geophysical Research* 96, 18,245–18,259.
- Pezzopane, S.K., Weldon II, R.J., 1993. Tectonic role of active faulting in central Oregon. *Tectonics* 12, 1140–1169.
- Pickering, G., Peacock, D.C.P., Sanderson, D.J., Bull, J.M., 1997. Modeling tip zones to predict the throw and length characteristics of faults. *American Association of Petroleum Geologists Bulletin* 81, 82–99.
- Reches, Z., 1978. Analysis of faulting in three-dimensional strain field. *Tectonophysics* 47, 109–129.
- Richard, P., 1991. Experiments on faulting in a two-layered cover sequence overlying a reactivated basement fault with oblique-slip. *Journal of Structural Geology* 13, 459–469.
- Rodgers, D.A., 1980. Analysis of pull-apart basin development produced by en echelon strike-slip faults. In: Balance, P.F., Reading, H.G. (Eds.), *Sedimentation in Oblique-slip Mobile Zones*. International Association of Sedimentologists Special Publication 4, pp. 27–41.
- Scott, D.L., Etheridge, M.A., Rosendahl, B.R., 1992. Oblique-slip deformation in extensional terrains; a case study of the lakes Tanganyika and Malawi rift zones. *Tectonics* 11, 998–1009.
- Segall, P., Pollard, D.D., 1980. Mechanics of discontinuous faults. *Journal of Geophysical Research* 85, 4,337–4,350.
- Simpson, G.D., 1990. Late Quaternary Tectonic Development of the North-western Part of the Summer Lake Basin, South-Central Oregon. M.S. thesis, Humboldt State University.
- Smith, J.V., Durney, D.W., 1992. Experimental formation of brittle structural assemblages in oblique divergence. *Tectonophysics* 216, 235–253.
- Stewart, J.H., Walker, G.W., Kleinhampl, F.J., 1975. Oregon–Nevada lineament. *Geology* 3, 265–268.
- Thomas, A.L., 1993. Poly3d: a three-dimensional, polygonal element, displacement discontinuity boundary element computer program with applications to fractures, faults and cavities in the earth's crust. M.S. thesis, Stanford University.
- Thompson, G.A., Burke, D.B., 1974. Regional geophysics of the Basin and Range Province. *Annual Review of Earth and Planetary Sciences* 2, 213–238.
- Trudgill, B., Cartwright, J., 1994. Relay-ramp forms and normal-fault linkages, Canyonlands National Park, Utah. *Geological Society of America Bulletin* 106, 1143–1157.
- Umhoefer, P.J., Stone, K.A., 1996. Description and kinematics of the SE Loreto Basin fault array, Baja California Sur, Mexico; a positive field test of oblique-rift models. *Journal of Structural Geology* 18, 595–614.
- Walker, G.W., Peterson, N.V., Greene, R.C., 1967. Reconnaissance geologic map of the east half of the Crecent Quadrangle, Lake, Deschutes, and Crook Counties, Oregon. U.S. Geological Survey Map I-493, scale 1:250,000.
- Wells, R.E., 1975. The geology of the Drake Peak rhyolite complex and the surrounding area, Lake County, Oregon. M.S. thesis, University of Oregon.
- Willemsse, E., 1997. Segmented normal faults: correspondence between three-dimensional mechanical models and field data. *Journal of Geophysical Research* 102, 675–692.
- Williams, A., 1958. Oblique-slip faults and rotated stress systems. *Geological Magazine* XCV, 207–218.
- Withjack, M.O., Jamison, W.R., 1986. Deformation produced by oblique rifting. *Tectonophysics* 126, 99–124.
- Zoback, M.L., Zoback, M.D., 1989. Tectonic stress field of the continental United States. *Geological Society of America Memoir* 172, 523–539.